Assessment of the Fractal Dimension of Images Derived by Biopsy of Pancreatic Tissue: Implications for Tumor Diagnosis

A. Scampicchio[1], A. Tura[2], S. Sbrignadello[2], F. Grizzi[3], S. Fiorino[4], S. Blandamura[5], and L. Finesso[6]

[1] Department of Information Engineering, University of Padova, Padova, Italy
[2] CNR Institute of Neuroscience, Padova, Italy
[3] Department of Inflammation and Immunology, Humanitas Clinical and Research Center, Rozzano, Milan, Italy
[4] UOSD Medicine C, Maggiore Hospital, AUSL Bologna, Bologna, Italy
[5] Department of Medicine, DIMED, University of Padova, Padova, Italy
[6] CNR Institute of Electronics, Computer and Telecommunication Engineering, Padova, Italy

Abstract— **Pancreatic tumors are characterized by marked deposition of extra-cellular matrix, also called desmoplasia, which interacts with tumor cells and facilitates the tumor onset and progression. Thus, it would be relevant to develop a method to quantitatively assess the amount of desmoplasia in images derived from bioptic tissue fragments of the pancreas. To this purpose, we applied the principles of fractal geometry, for the assessment of the fractal dimension of images of Masson's trichrome stained pancreatic tissue. Thus, we implemented an algorithm for the computation of the Hausdorff dimension, based on the box counting method: the image is split into boxes of identical size, and the number of boxes needed to cover the features of interest in the image is counted. The process is then iterated with boxes of lower size, and finally all box counts obtained at the different steps are considered, to get the estimate of the Hausdorff dimension, *D*. After validating the algorithm with appropriate tests, we applied it to pancreatic images, where some regions of interest (ROI) were identified, including both healthy and non-healthy (fibrotic) tissue. We found that non-healthy ROI typically show higher *D* values than healthy ROI (1.927±0.086 vs. 1.750±0.070 (mean±SD), p=0.0013). Thus, our approach may be of help for an accurate quantification of the degree of severity of pancreatic tumors.**

Keywords— **Hausdorff-Besicovitch dimension, Hurst exponent, desmoplasia, adenocarcinoma, image processing.**

I. Introduction

Pancreatic tumors are characterized by marked desmoplastic reaction. In fact, activated pancreatic stellate cells, which are the main source of extracellular-matrix (ECM) in the microenvironment, strongly interact with tumor cells, thus facilitating tumor growth [1]. Thus, it would be relevant to develop a method for automated, quantitative assessment of the amount of ECM in images derived by biopsy of the pancreatic tissue. This would be of help for evaluation of the degree of severity of pancreatic tumors.

The ECM consists of a complex set of irregularly shaped fragments, thus the Euclidean metric appears inadequate to describe such kind of shapes [2]. To this purpose, a more appropriate approach may be the fractal geometry. Indeed, fractal geometry was introduced by Benoit Mandelbrot some decades ago [3], and it was subsequently proposed to apply it in the field of human physiology and pathology [4-8].

In this study, we apply the principles of fractal geometry for the assessment of the fractal dimension of images derived by pancreatic tissue and treated by Masson's trichrome stain [9, 10]. Our aim was to explore the potential of fractal dimension assessment to discriminate between normal and tumor tissue.

II. Materials and Methods

A. The Concept of Fractals

The concept of fractal object was introduced by Mandelbrot [3], which aimed to provide the basis of a new geometry that was appropriate for the analysis of irregular, even chaotic phenomena, whose study through traditional geometry was not sufficiently accurate for the typical applications. In this study, we focus on one of the main properties of the fractal objects, that is, the fractal (non-integer) dimension. More specifically, we developed an algorithm for the calculation of the Hausdorff (also called Hausdorff-Besicovitch) dimension [11, 12].

B. Box Counting Algorithm

The direct calculation of the Hausdorff dimension for biological fractal objects can be difficult (such objects often do not display a specific homothety ratio), and hence an approximated calculation is performed. Three main methods have been proposed for this purpose: *i)* cluster growing [13, 14]; *ii)* correlation analysis [15, 16]; *iii)* box counting [17, 18]. In this study, we focused on the box counting method. The Hausdorff fractal dimension, *D*, is calculated as:

$$D = \lim_{\varepsilon \to 0} \inf \frac{\log\left(N(\varepsilon)\right)}{\log\left(1/\varepsilon\right)}$$

E. Kyriacou et al. (eds.), *XIV Mediterranean Conference on Medical and Biological Engineering and Computing 2016*,
IFMBE Proceedings 57,
DOI: 10.1007/978-3-319-32703-7_77

Where ε is the length of the box side, and $N(\varepsilon)$ is the minimum number of boxes necessary to cover the surface of interest.

The flow chart of the method is reported in Figure 1.

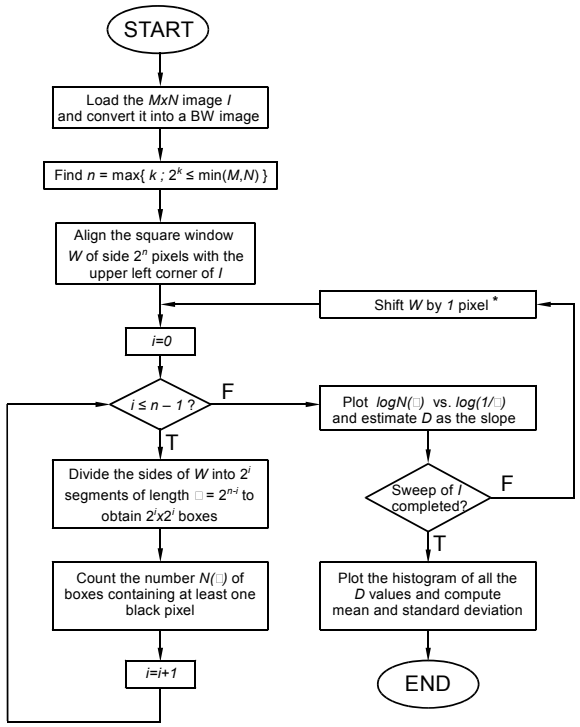

** Shift the window W one pixel at a time, sweeping the image I left to right and top to bottom*

Fig. 1 Flow chart of the method for calculation of the fractal dimension.

The algorithm splits the image of interest into boxes. Then, the number of boxes, which are necessary for image covering, and which contain useful information, is counted. The process is iterated for decreasing ε values, and the angular coefficient of the regression line of $\log(N(\varepsilon))$ versus $\log(1/\varepsilon)$ is eventually computed. Since at each step the covering boxes are of equal size, an approximation of the Hausdorff fractal dimension is obtained.

More specifically, our algorithm is based on the following steps:

i) Load the image of interest;

ii) Convert it into black and white: the black part should represent the component containing information of interest, that is, regions with ECM (some details are reported in one of the next sections);

iii) Find one sub-image, entirely included in the original image, with the biggest possible size, but of square type, i.e., its number of pixels per side is a power of 2 (let's call *n* that power);

iv) For *i* from *0* to *n-1*, divide every side of the square image into 2^i segments of length $\varepsilon=2^{n-i}$, in order to obtain $2^i \times 2^i$ subfigures, which are the boxes;

v) Count the number of boxes containing at least one pixel of information (0-valued pixel, i.e., black);

vi) Defining $N(\varepsilon)$ as the number of counted boxes of side ε, plot the function $\log(N(\varepsilon))/\log(1/\varepsilon)$;

vii) Estimate the slope of the plot indicated above, and assume it as the estimate of *D*;

viii) Repeat the procedure indicated in steps *iv)* to *vii)* for all the possible square sub-images in the original image (see step *iii)*), and save the corresponding *D* values obtained;

ix) Plot the histogram of all the *D* values;

x) Assuming the histogram as the density function of *D*, compute its mean and standard deviation.

The described algorithm was implemented under MATLAB® environment (The MathWorks, Inc., USA).

C. Algorithm Validation

Several tests were performed to assess the accuracy of the algorithm, based on black and white images generated randomly or taken from the scientific literature. Among the most relevant tests, we mention the test performed on the Sierpinski carpet [19] (Figure 2).

In fact, for such image the fractal dimension can be computed theoretically, and equals $\log_3 8$ (approx. 1.8928). Our algorithm applied to the finite approximations of the Sierpinski carpet returns fractal dimension 1.9015±0.0081 for the 4 iterations approximation, and 1.8454±0.0221 for the 5 iterations approximation, in good agreement with the theoretical value.

D. Analyses of Images of Masson's Trichrome Stained Pancreatic Tissue

Masson's trichrome stain is a widely used histochemical staining method to highlight the presence of ECM (thus allowing the identification of the regions with possible desmoplastic reaction). Collagen is in fact colored in green or cyan. Instead, parenchymal tissue (that is, the residual functional tissue) assumes brown color.

An example of Masson's trichrome stained tissue is shown in Figure 3. It reports a wide portion of the pancreatic biopsy, with tissues in different conditions.

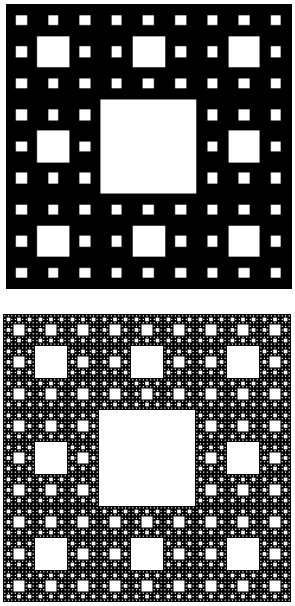

Fig. 2 Sierpinski carpet, obtained with three (top) and five (bottom) iterations of the corresponding generating algorithm.

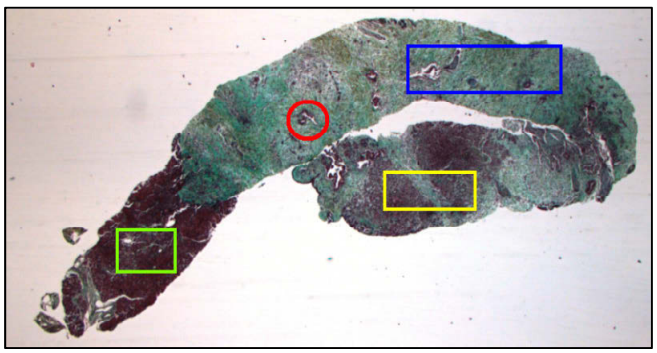

Fig. 3 Masson's trichrome-based image of pancreatic tissue, with indication of different regions: healthy parenchymal tissue (green), ductal parenchymal tissue with fibrosis in the normal range (yellow), neoplastic tissue with marked development of fibrosis (blue), neoplastic gland (red).

The assessment of the fractal dimension as described in the previous sections requires black and white images. Therefore, the Masson's trichrome-based images need to be properly transformed. To this purpose, some *ad-hoc* image functions were developed based on two possible strategies:

i) The image of interest is converted from Red-Green-Blue (RGB) format into grey scale format. Subsequently, the gray scale image is inspected pixel-by-pixel, and each pixel is assigned to black (0-value) or white (255-value) color, based on the comparison with a threshold, empirically identified to discriminate between useful or not-useful image information.

ii) The image of interest is converted directly from RGB format into black and white format, based on empirical ranges again empirically identified. Our tests showed that the approach *ii)* provided the best results, thus it was chosen. Selected RGB ranges providing black pixels were 55-203, 140-235, 120-255 for red, green, blue, respectively.

In this study, we analyzed images from six patients (average age 65 yr), which provided informed consent for biopsy execution. Each image derived from the acquisition through microscopy (at 5x objective magnification) of the biopsy pancreatic tissue. For each image, the pathologist manually identified four regions (ROI), considered well representing the tissue in a specific state, including fibrosis at different degree of deposition, and natural (i.e., healthy) parenchyma. For each ROI, fractal dimension estimate was performed.

III. Results

All tests performed for the validation of the algorithm confirmed its reliability. As regards the tests on Sierpinski carpet, for the image derived by five iterations (see Figure 2, bottom) we obtained $D = 1.8454 \pm 0.0221$, which is close to the theoretical value of the carpet.

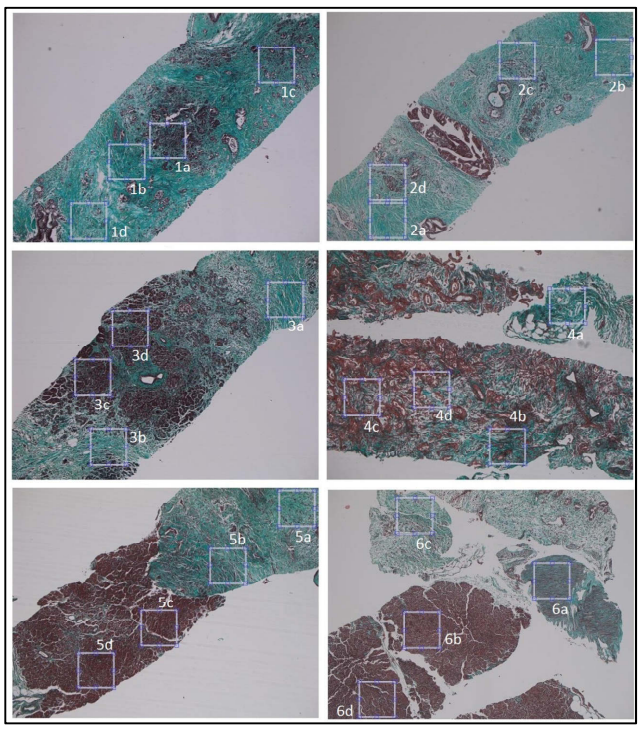

Fig. 4 The analyzed Masson's trichrome-based images of pancreatic tissues, with four regions of interest (ROI) selected in each image. Image order (1-6) is left to right, then top to bottom.

Figure 4 shows the six pancreatic images with the indication of the selected ROI for each image.

ROI were classified into the following categories:

Type i) Fibrosis;
Type ii) Fibrosis with neoplastic glands;
Type iii) Fibrosis and parenchyma;
Type iv) Fibrosis with traces of parenchyma;
Type v) Natural parenchyma;
Type vi) Natural parenchyma with blood vessels;
Type vii) Parenchyma with only traces of fibrosis.

An example of histogram for the computed values of the fractal dimension *D* for each ROI is reported in Figure 5.

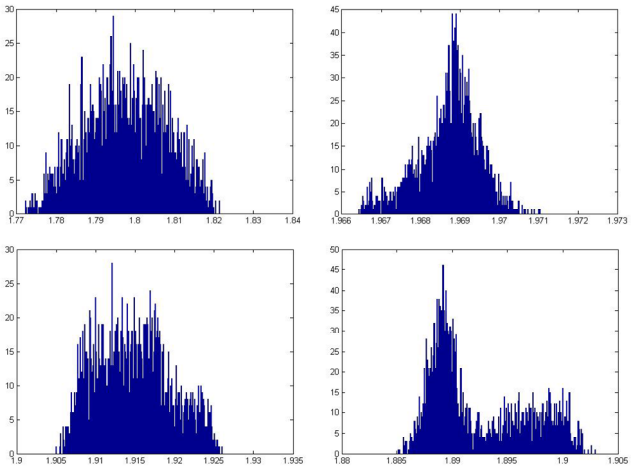

Fig. 5 Histogram of the *D* values for ROI *a* (top, left), *b* (top, right), *c* (bottom, left), *d* (bottom, right), for image 1.

Figure 6 reports the same plot but with equal x-axis scale for easier comparison.

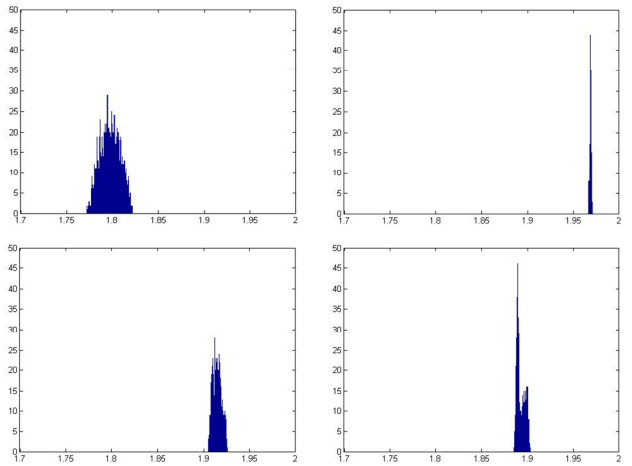

Fig. 6 Histogram of the *D* values for ROI *a* (top, left), *b* (top, right), *c* (bottom, left), *d* (bottom, right), for image 1 , with the same x-axis scale.

Table 1 reports the classification of the different ROI of the six images, with the corresponding *D* value.

Table 1 Classification (histology) and *D* value of the image ROI

Image and ROI	Classification	*D* value (mean±SD)
1a	Parenchyma with traces of fibr.	1.7976±0.0104
1b	Fibrosis	1.9687±7.8484e-04
1c	Fibrosis and parenchyma	1.9148±0.0047
1d	Fibrosis	1.8924±0.0044
2a	Fibrosis	1.9902±4.8633e-04
2b	Fibrosis	1.9930±7.3133e-04
2c	Fibrosis with traces of par.	1.9930±7.3133e-04
2d	Fibrosis with traces of par.	1.9587±7.3842e-04
3a	Fibrosis	1.97122±0.0014
3b	Fibrosis	1.9433±0.0028
3c	Healthy parenchyma	1.7697±0.0057
3d	Parenchyma with traces of fibr.	1.85607±0.0031
4a	Fibrosis	1.9241±0.0056
4b	Fibrosis	1.9095±0.0052
4c	Fibrosis with neoplastic glands	1.7592±0.0045
4d	Fibrosis with neoplastic glands	1.6709±0.0079
5a	Fibrosis	1.9639±0.0019
5b	Fibrosis	1.9681±0.0013
5c	Natural parenchyma	1.7634±0.0051
5d	Natural parenchyma	1.7342±0.0098
6a	Fibrosis and parenchyma	1.9713±0.0013
6b	Natural parenchyma	1.6703±0.0087
6c	Fibrosis	1.9611±0.0015
6d	Natural parenchyma with vessels	1.6564±0.0021

By inspection of the table, it can be noticed that ROI with fibrosis tend to display higher *D* values. When grouping all the ROI with some degree of fibrosis (i.e., *types i)-iv)*) into a unique category (fibrotic tissue), and similarly for ROI with natural (or almost natural) parenchyma (i.e., *types v)-vii)*: non-fibrotic tissue), by considering the mean *D* values in each ROI, a statistically significant difference was found between fibrotic and non-fibrotic tissue (1.927±0.086 and 1.750±0.070 (mean±SD), p=0.0013, according to non-parametric Mann-Whitney test).

IV. DISCUSSSION

In this study, we estimated the fractal dimension of images derived by pancreatic biopsy, whose tissue was treated with the Masson's trichrome stain. We found that images related to tissue with fibrosis display higher values of the fractal dimension, as it can be appreciated from the example

histogram of Figure 6 and by inspection of Table 1, and confirmed by the statistical testing.

Comparison with previous studies is difficult. In fact, fractal dimension analysis was previously applied to images of different organs rather than pancreas, such as brain tumors [7, 8] or the liver [20, 21]. As regards pancreatic tissues, to our knowledge, only two previous studies performed fractal analyses [22, 23]. However, in study [22], the focus was on the analysis of the fractal microvascular morphology, rather than the analysis of desmoplastic reaction in the pancreatic microenvironment. Also, experiments were performed on animals and not on human tissues. In study [23], focus was again partially different than in our study, since the fractal analysis was applied for the assessment of nuclear shape and chromatin distribution of the pancreatic cells. Moreover, study [23] aimed to distinguish between resectable and non-resectable tumors, thus analyses and comparisons with natural tissue (which is important for a full validation of the fractal approach) were missing. Furthermore, the tissues were not treated with the Masson's trichrome stain, but with other techniques. Nonetheless, it can be noticed that non-resectable (i.e., more advanced) tumors showed higher fractal dimensions than resectable tumors, and this is essentially in agreement with our results.

Our study has some limitations that need to be addressed in future studies. In fact, a larger image dataset should be analyzed, with the purpose to evaluate the actual potential of the approach not only to distinguish between natural and diseased tissues, but also to classify the severity of a tumor, in combination with other clinical parameters. Also, an automated algorithm should be developed for appropriate selection of the regions where fractal analysis has to be carried out, to replace the manual (i.e., partially subjective) selection performed in this study. For binarization of the images automatic segmentation methods will also be considered. Furthermore, performance of our approach on images at higher level of magnification should be tested. Finally, comparison should be performed with other staining approaches used in histology, such as the Picrosirius red [24], which represents another technique to detect the presence of ECM.

V. Conclusions

We implemented an algorithm for calculating the fractal dimension of pancreatic biopsy derived images, based on Masson's trichrome stain. We found that images related to tissue with fibrosis display higher levels of the fractal dimension. This may be useful for improved accuracy in the staging of pancreatic tumors.

Conflict of Interest

The authors declare that they have no conflict of interest.

References

1. Apte M, Pirola RC, Wilson JS (2015) Pancreatic stellate cell: physiologic role, role in fibrosis and cancer. Curr Opin Gastroenterol 31: 416–423 DOI 10.1097/MOG.0000000000000196
2. Dioguardi N, Grizzi F, Franceschini B, Bossi P, Russo C (2006) Liver fibrosis and tissue architectural change measurement using fractal-rectified metrics and Hurst's exponent. World J Gastroenterol 12:2187–2194
3. Mandelbrot B (1967) How long is the coast of Britain? Statistical self-similarity and fractional dimension. Science 156:636–638
4. West BJ (1990) Physiology in fractal dimensions: error tolerance. Ann Biomed Eng 18:135–149
5. Glenny RW, Robertson HT, Yamashiro S, Bassingthwaighte JB (1991) Applications of fractal analysis to physiology. J Appl Physiol 70:2351–2367
6. Cross SS (1997) Fractals in pathology. J Pathol 182:1-8
7. Di Ieva A, Grizzi F, Jelinek H, Pellionisz AJ, Losa GA (2013) Fractals in the neurosciences, Part I: general principles and basic neurosciences. Neuroscientist 20:403-417
8. Di Ieva A, Esteban FJ, Grizzi F, Klonowski W, Martín-Landrove M (2015) Fractals in the neurosciences, Part II: clinical applications and future perspectives. Neuroscientist 21:30-43
9. Schaefer HJ (1957) A rapid trichrome stain of Masson type. Am J Clin Pathol 28:646–647
10. Cohen AH (1976) Masson's trichrome stain in the evaluation of renal biopsies. An appraisal. Am J Clin Pathol 65:631–643
11. Eden A (1990) Local estimates for the Hausdorff dimension of an attractor. J Math Anal Appl 150:100–119 DOI 10.1016/0022-247X(90)90198-O
12. Mattila P (2004) Hausdorff dimension, projections, and the Fourier transform. Publ Mat 48:3–48
13. Keyes T, Seeley G, Weakliem P, Ohtsuki T (1987) Collision-induced light scattering from growing clusters. Depolarization by fractals. J Chem Soc, Faraday Trans 2 83:1859–1866 DOI 10.1039/F2987 8301859
14. Mandelbrot BB, Evertsz CJG (1990) The potential distribution around growing fractal clusters. Nature 348:143–145
15. Lin DC, Sharif A (2007) Wavelet transform modulus maxima based fractal correlation analysis. Eur Phys J B 60:483–491 DOI 10.1140/epjb/e2008-00004-6
16. Santolalla C, Chavez-Esquivel G, Reyes-Heredia JADL, Alvarez-Ramirez J (2013) Fractal correlation analysis of x-ray diffraction patterns with broad background. Ind Eng Chem Res 52:8346–8353 DOI 10.1021/ie303069y
17. Mainieri R (1993) On the equality of Hausdorff and box counting dimensions. Chaos 3:119–126
18. Dai M, Liu X (2008) The Hausdorff and box-counting dimensions of a class of recurrent sets. Chaos Soliton Fract 36:532–538 DOI 10.1016/j.chaos.2006.06.083

19. Ebrahimi Khabbazi A, Hinebaugh J, Bazylak A (2015) Analytical tortuosity-porosity correlations for Sierpinski carpet fractal geometries. Chaos Soliton Fract 78:124–133 DOI 10.1016/j.chaos.2015.07.019
20. Dioguardi N, Grizzi F, Franceschini B, Bossi P, Russo C (2006) Liver fibrosis and tissue architectural change measurement using fractal-rectified metrics and Hurst's exponent. World J Gastroenterol 12:2187–2194
21. Dioguardi N, Grizzi F, Fiamengo B, Russo C (2008) Metrically measuring liver biopsy: a chronic hepatitis B and C computer-aided morphologic description. World J Gastroenterol 14:7335–7344
22. Lin KY, Maricevich M, Bardeesy N, Weissleder R, Mahmood U (2008) In vivo quantitative microvasculature phenotype imaging of healthy and malignant tissues using a fiber-optic confocal laser microprobe. Transl Oncol 1:84–94
23. Vasilescu C, Giza DE, Petrisor P, Dobrescu R, Popescu I, Herlea V (2012) Morphometrical differences between resectable and non-resectable pancreatic cancer: a fractal analysis. Hepatogastroenterol 59:284–288 DOI 10.5754/hge11277
24. Constantine VS, Mowry RW (1968) Selective staining of human dermal collagen. II. The use of picrosirius red F3BA with polarization microscopy. J Invest Dermatol 50:419–423

Author:	Lorenzo Finesso
Institute:	CNR IEIIT
Street:	Via Gradenigo 6/B
City:	Padova
Country:	Italy
Email:	lorenzo.finesso@ieiit.cnr.it